Experimental and Computational Studies of Alkali-Metal Coinage-Metal Clusters

Ying-Chan Lin and Dage Sundholm*

Department of Chemistry, P.O. Box 55 (A.I. Virtanens plats 1), FIN-00014 University of Helsinki, Finland

Jonas Jusélius*

Department of Chemistry, University of Tromsø, N-9037 Tromsø, Norway

Li-Feng Cui, Xi Li, Hua-Jin Zhai, and Lai-Sheng Wang*

Department of Physics, Washington State University, 2710 University Drive, Richland, Washington 99352 and W. R. Wiley Environmental Molecular Sciences Laboratory and Chemical Sciences Division, Pacific Northwest National Laboratory, MS K8-88, P.O. Box 999, Richland, Washington 99352

Coinage and alkali metal mixed clusters, M_4Na^- (M = Cu, Au) have been investigated experimentally using photoelectron spectroscopy and computationally at correlated ab initio levels. The related Cu_4Li^-, Ag_4Li^-, Ag_4Na^-, and Au_4Li^- clusters as well as the neutral Cu_4Li_2 and Cu_4Na_2 clusters have also been studied computationally. The calculations show that the two lowest isomers of the negatively charged clusters include a pyramidal C_{4v} structure and a planar C_{2v} species. For Cu_4Li^- and Cu_4Na^-, the C_{4v} structure is calculated at correlated ab initio level to be 30.9 and 16.9 kJ/mol below the planar C_{2v} isomer, whereas the planar isomers of Au_4Li^- and Au_4Na^- are found to be 29.7 and 49.4 kJ/mol below the pyramidal ones. For Ag_4Li^- and Ag_4Na^-, the pyramidal isomers are the lowest ones. Comparison of the calculated and measured photoelectron spectra of Cu_4Na^- and Au_4Na^- shows that the pyramidal Cu_4Na^- cluster of C_{4v} symmetry and the planar Au_4Na^- of C_{2v} symmetry are detected experimentally. Calculations of the magnetically induced current density in Cu_4Li^- and Cu_4Li_2 using the Gauge-Including Magnetically Induced Current (GIMIC) method show that strong ring currents are sustained mainly by the highest-occupied molecular orbital primarily derived from the Cu 4s. The GIMIC calculations thus show that the Cu_4^{2-} ring is σ-aromatic and that the *d* orbitals do not play any significant role for the electron delocalization effects. The present study does not support the notion that the square-planar Cu_4^{2-} is the first example of *d*-orbital aromatic molecules.

I. Introduction

Photoelectron spectroscopy (PES) and ab initio calculations have recently been used to study a series of ring-shaped metal clusters consisting of planar four-membered molecular rings, which are shown to be stabilized by cyclic electron delocalization or aromaticity.[1−8] The aromatic nature of these ring-shaped metal clusters has been subsequently studied and confirmed.[9−14] The generally accepted notion is that ring-shaped metal clusters with $(4n + 2)\pi$ electrons such as Al_4^{2-} and Hg_4^{6-} can be aromatic and that they sustain ring currents when exposed to external magnetic fields, similar to ordinary aromatic molecules. Explicit calculations of the magnetically induced current densities have shown that for Al_4^{2-}, both σ and π orbitals sustain diatropic (aromatic) ring currents, whereas for Al_4^{4-} species the current is σ diatropic (aromatic) and the π current is paratropic (antiaromatic). This notion is also supported by earlier calculations of nucleus independent chemical shifts (NICS).[15] Thus, new concepts of multiple aromaticity for metal clusters, such as σ and π aromaticity, and σ aromaticity and π antiaromaticity, have been introduced. A recent study of the magnetically induced currents of Al_4^{2-} and Al_4^{4-} using the Gauge-Including Magnetically Induced Current (GIMIC) method[16] yielded explicit values for the ring-current strengths, as well as the diatropic (aromatic) and paratropic (antiaromatic) contributions to the ring current.[14] The ring-current study of the Al_4 clusters also provided accurate information about the shape of the magnetically induced ring currents and the aromaticity properties of the controversial case of Al_4^{4-} [17] can now be considered understood:[14] it is π-antiaromatic and σ-aromatic as originally suggested.[2]

Wannere et al.[18] recently studied computationally four-membered ring species of coinage metals, such as bipyramidal Cu_4Li_2, Ag_4Li_2, and Au_4Li_2 clusters of D_{4h} symmetry and used NICS calculations to assess their aromaticity. In these cases, Wannere et al.[18] found that the largest diamagnetic (aromatic) contribution to the NICS value originates from the a_{1g} molecular orbital (MO), which is built mainly from the 4s atomic orbitals (AOs). However, the paramagnetic (antiaromatic) contribution from the highest occupied e_u orbitals, also formed mainly by the 4s AOs, cancels the a_{1g} contribution. Thus, the diamagnetic NICS value of −14.5 ppm seems to originate from the MOs with mainly 3d character. They considered therefore these coinage-alkali metal clusters as the first example of *d*-orbital aromatic molecules.[18]

We also mention here the recent density-functional theory (DFT) study by Fuentealba and Padilla-Campos[19] who calculated the molecular structures of neutral and positively charged

* To whom correspondence should be addressed. Email: sundholm@chem.helsinki.fi. E-mail: jonas.juselius@chem.uit.no. E-mail: ls.wang@pnl.gov.

Alkali-Metal Coinage-Metal Clusters

J. Phys. Chem. A, Vol. 110, No. 12, 2006 **4245**

bimetallic Cu_mLi_n (m, $n \leq 4$) clusters as well as the DFT studies by Tsipis et al.[20,21] who proposed a new class of molecules consisting of planar cyclic copper hydrides, Cu_nH_n.

In the present work, we report the generation of Cu_4Na^- and Au_4Na^- clusters in the gas phase and their characterization experimentally using photoelectron spectroscopy and computationally at correlated ab initio levels. The singly charged M_4Li^- (M = Cu, Ag, Au) and Ag_4Na^- species as well as the neutral Cu_4Li_2 and Cu_4Na_2 clusters have also been considered in the theoretical study. Photoelectron spectra of Cu_4Na^- and Au_4Na^- have been simulated by equation-of-motion coupled-cluster calculations of the low-lying electron detachment transitions and compared with the experimental data to identify the clusters observed in the PES experiment. The electron delocalization and aromaticity properties were studied by performing explicit calculations of the magnetically induced current densities using the newly developed GIMIC method.[16] Numerical integration of the magnetically induced current densities provided information about the ring-current strengths and the shape of the ring current. The GIMIC calculations clearly demonstrated that the square-planar coinage metal M_4^{2-} clusters are σ-aromatic systems primarily due to the s orbital bonding.

II. Experimental and Computational Methods

A. Experimental Methods. The experiments were carried out using a magnetic-bottle PES spectrometer, details of which have been described elsewhere.[22,23] Coinage-metal/sodium alloy clusters were produced by laser vaporization of compressed disk targets made from M (M = Cu, Au) and Na. The laser-produced plasma was mixed with a helium carrier gas pulse at 10 atm backing pressure. A cold cluster beam was produced by a supersonic expansion of the cluster/carrier gas mixture through a 2 mm diam nozzle and collimated by a 6 mm diam skimmer. The anions were extracted from the beam perpendicularly and separated by a time-of-flight mass spectrometer. The M_4Na^- (M = Cu, Au) cluster anions of interest were selected and decelerated before crossing with a detachment laser beam in the interaction zone of the magnetic-bottle PES analyzer. Photoelectrons were collected at nearly 100% efficiency by the magnetic-bottle and analyzed in a 3.5-m long electron flight tube. The spectra were calibrated with the known spectra of Cu^- and Au^-. The apparatus has an electron energy ($\Delta E/E$) resolution of ~2.5%, i.e., about 25 meV for photoelectrons of 1 eV kinetic energy.

B. Computational Methods. The molecular structures were optimized at the second-order Møller–Plesset perturbation level (MP2) using the TURBOMOLE program package.[24] The stationary points obtained in the structure optimizations were checked by calculating the vibrational frequencies numerically using finite differences. For Li, Na, Cu, and Ag, the Karlsruhe standard triple-ζ valence basis sets augmented with double polarization functions (TZVPP) were used. For gold, we employed the Karlsruhe Au basis set consisting of $7s5p3d$ basis functions[25] augmented with $2f$ as suggested by Pyykkö et al.[26] The $7s5p3d$ basis set has been optimized for the neutral gold trimer[25] and has proven to be cost efficient yielding accurate energies for gold species. Furche et al.[25] found that the addition of a p function with an exponent of about 0.8 is necessary for an accurate description of gold clusters.[27] For Ag and Au, the effective core potentials (ECP) from the Stuttgart group[28] were employed. The small-core ECP replaces 60 of the core electrons, and thus 19 electrons per gold atom were considered in the calculations. For Ag, also 19 electrons were considered thus replacing 28 core electrons with the ECP. In the correlation
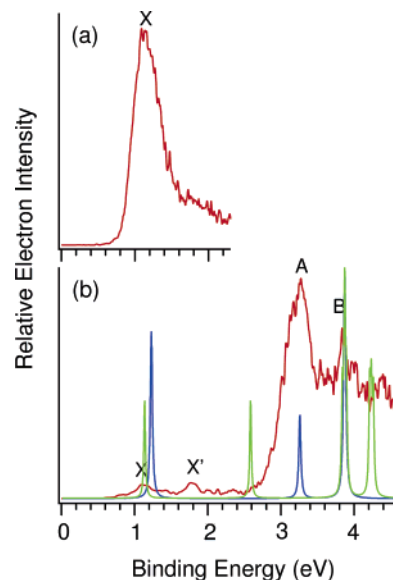

Figure 1. Comparison of calculated and measured photoelectron spectra of Cu_4Na^-. The measured spectra taken at (a) 532 nm (2.331 eV) and (b) 266 nm (4.661 eV) are shown in red. The calculated spectrum for the C_{4v} isomer is shown in blue and the spectrum of the planar C_{2v} isomer in green.

calculations on the Cu_4^{2-} species, ten of the Cu electrons and two of the Na electrons were uncorrelated, whereas for the Ag and Au clusters all considered electrons were correlated. Single-point MP2 calculations using the Karlsruhe quadruple-ζ valence basis sets augmented with double sets of polarization functions (QZVPP) were employed to check the basis-set convergence of the isomer energy differences.

The photoelectron spectra were calculated at the coupled-cluster singles and doubles (CCSD) level using the equation-of-motion ionization-potential (EOMIP) formalism.[29] The coupled-cluster calculations were performed with the Austin-Mainz version of the ACES II program package.[30] The same basis sets as used in the structure optimizations were employed in the EOM calculations of the vertical detachment energies.

The nuclear magnetic shieldings and magnetically induced current densities for Cu_4Li^- and Cu_4Li_2 were calculated at the CCSD level using ACES II.[31–34] The magnetically induced current densities were deduced from the one-particle density matrix, the magnetically perturbed density matrixes obtained in the shielding calculations, and basis-set information using the Gauge-Including Magnetically Induced Current (GIMIC) approach.[16] The GIMIC method has been described in detail in ref 16.

III. Experimental Results

The measured photoelectron spectra of Cu_4Na^- taken at two laser wavelengths, 532 nm (2.331 eV) and 266 nm (4.661 eV) are shown with the red curves in Figure 1. The photoelectron spectra of Au_4Na^- recorded at three laser wavelengths are analogously shown in Figure 2. The 266 nm spectrum of Cu_4Na^- displayed two weak bands (X, X') at lower binding energies and two strong bands (A, B) at higher energies. The X' band at 1.8 eV almost completely disappeared in the 532 nm spectrum and was most likely due to a mass contamination. The X band represents the transition from the ground state of Cu_4Na^- to that of Cu_4Na, yielding adiabatic (ADE) and vertical (VDE) detachment energies of 0.83 and 1.13 eV, respectively. The broad peak of the X band suggests a significant geometry change between the ground states of Cu_4Na^- and Cu_4Na. The
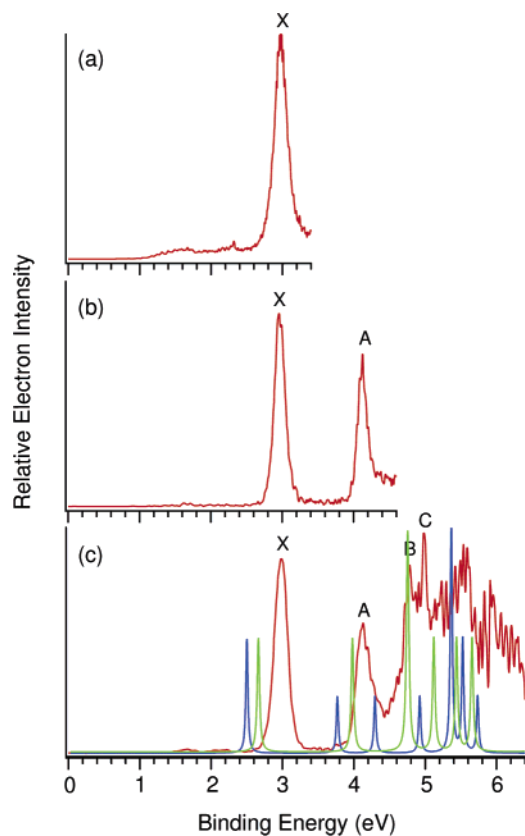
Figure 2. Comparison of calculated and measured photoelectron spectra of Au_4Na^-. The measured spectra taken at (a) 355 nm (3.496 eV), (b) 266 nm (4.661 eV), and (c) 193 nm (6.4244 eV) are shown in red. The calculated spectrum for the C_{4v} isomer is shown in blue and the spectrum of the planar C_{2v} isomer in green.

A band in Figure 1b corresponding to a VDE of 3.26 eV and the B band (VDE: 3.84 eV) represent detachment transitions to two excited states of Cu_4Na. Other weak features are also present on the higher binding energy side of the 266 nm spectrum, giving the congested appearance in this spectral range. The weak features are also most likely due to the contaminant associated with band X′.

The experimental photoelectron spectra of Au_4Na^- in Figure 2 show no resemblance to those of Cu_4Na^-. Au_4Na^- seems to have much higher electron binding energies. Its ground state transition defined by band X yielded ADE and VDE of 2.82 and 2.98 eV, respectively. Three excited state transitions (A, B, C) were clearly resolved at VDEs of 4.12, 4.79, and 4.98 eV, respectively. Higher binding energy features in the 193 nm spectrum were observed but not well resolved. The Au_4Na^- spectra appear to have less contamination problems. The weak and broad features at lower binding energies (1.2 to 2.6 eV) in Figure 2a could be due to contamination or due to the presence of other low-lying isomers, but the 266 and 193 nm spectra shown in Figures 2b and 2c were quite clean.

The observed ADEs and VDEs are summarized in Table 1. To elucidate the structure and bonding of the two coinage alkali mixed clusters, the experimental data will be compared to calculated ionization potentials in Section 4.2.

IV. Theoretical Results and Discussions

A. Molecular Structures. The energetically lowest structure obtained in the MP2/TZVPP optimization of Cu_4Li_2 is a bipyramidal cluster of D_{4h} symmetry (Figure 3a). At this computational level, it lies 77.0 kJ/mol below the planar one

TABLE 1: The Observed Vertical Electron Detachment Energies (VDE in eV) from the Photoelectron Spectra of Cu_4Na^- in Figure 1 and Au_4Na^- in Figure 2. the Uncertainty Is ± 0.05 eV

species	X[a]	A	B	C
Cu_4Na^-	1.13	3.26	3.84	
Au_4Na^-	2.98	4.12	4.79	4.98

[a] The adiabatic detachment energies for the X band or the electron affinities for the corresponding neutral Cu_4Na and Au_4Na are measured as 0.83 ± 0.04 and 2.82 ± 0.04 eV, respectively.
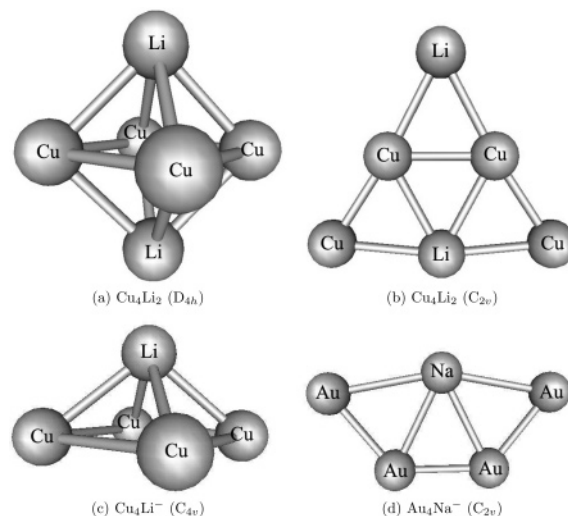

Figure 3. The molecular structure of (a) Cu_4Li_2 (D_{4h}), (b) Cu_4Li_2 (C_{2v}), (c) Cu_4Li^- (C_{4v}), and (d) Au_4Na^- (C_{2v}) optimized at the MP2 level using TZVPP (Cu, Li, Na) and $7s5d3d2f$ (Au) basis sets. The pictures have been made using gOpenMol.[43,44]

of C_{2v} symmetry (Figure 3b). The Cu atoms in Cu_4Li_2 seems to prefer to form a square with equidistant Cu−Cu bonds as previously reported.[18]

At the MP2/TZVPP level, the singly charged Cu_4Li^- cluster of C_{4v} in Figure 3c is found to be 11.7 kJ/mol below the planar C_{2v} isomer. The corresponding Au_4Na^- isomer of C_{2v} symmetry is shown in Figure 3d. However, the energy difference is small and by changing the counterion from Li^+ to Na^+ the pyramidal C_{4v} and the planar C_{2v} structures become almost degenerate with the planar structure 3.3 kJ/mol below the C_{4v} one. The planar isomer is stabilized further by inclusion of higher-order electron correlation effects. In single-point CCSD/TZVPP and CCSD-(T)/TZVPP calculations using the MP2/TZVPP structures, the planar isomer of Cu_4Li^- is 16.4 and 3.1 kJ/mol below the pyramidal one. For Cu_4Na^-, the planar isomer is 3.4, 31.0, and 17.1 kJ/mol below the pyramidal structure calculated at the MP2, CCSD, and CCSD(T) levels. Zero-point energy corrections and entropy contributions do not change the order of the isomers since they reduce the energy difference between the planar and pyramidal isomers by only a few kJ/mol. However, at the MP2/QZVPP level the pyramidal Cu_4Li^- and Cu_4Na^- clusters are 45.7 and 30.2 kJ/mol below the planar isomers yielding extrapolated CCSD(T)/QZVPP isomer energies of 30.9 and 16.9 kJ/mol for Cu_4Li^- and Cu_4Na^-, respectively. Thus, we conclude that for the singly charged Cu_4Li^- and Cu_4Na^- clusters, the pyramidal isomers of C_{4v} symmetry are the energetically lowest ones.

The lowest isomer of Cu_4Na_2 is the bipyramidal cluster of D_{4h} symmetry. At the MP2/TZVPP level it is found to be only 15.4 kJ/mol below the planar structure of C_{2v} symmetry. As for Cu_4Na^-, the use of the QZVPP basis set favors the bipyramidal isomer, whereas high-order electron correlation

Alkali-Metal Coinage-Metal Clusters

J. Phys. Chem. A, Vol. 110, No. 12, 2006 **4247**

TABLE 2: The Relative Isomer Energies (in kJ/mol) of the Planar (C_{2v}) M_4A^- (M = Cu, Ag, and Au; A = Li and Na) Isomers Calculated at the MP2, CCSD, and CCSD(T) Levels Using the TZVPP (Li, Na, Cu, and Ag) and 7s5p3d2f (Au) Basis Sets[a]

species	MP2	CCSD	CCSD(T)	CCSD(T)[b]
Cu_4Li^-	11.7	−16.4	−3.1	30.9
Cu_4Na^-	−3.5	−31.0	−17.1	16.9
Ag_4Li^-	12.4	−11.3	−3.5	−
Ag_4Na^-	−3.0	−28.0	−18.8	−
Au_4Li^-	0.6	−41.3	−29.7	−
Au_4Na^-	−17.9	−63.1	−49.4	−

[a] The molecular structures were optimized at the MP2 level using the same basis sets. Negative isomer energies indicate that the planar isomer is the lowest one. [b] Extrapolated CCSD(T)/QZVPP value.

contributions decrease the energy of the planar isomer relative to the bipyramidal one. At the extrapolated CCSD(T)/QZVPP level, the bipyramidal Cu_4Li_2 and Cu_4Na_2 clusters are found to be 99.8 and 54.5 kJ/mol below the planar ones.

The relative isomer energies of the Ag_4^{2-} clusters are very similar to those of the corresponding Cu species. At the MP2/TZVPP level, pyramidal Ag_4Li^- is 12.4 kJ/mol below the planar one, whereas at the CCSD/TZVPP and CCSD(T)/TZVPP levels, the planar isomer is 11.3 and 3.5 kJ/mol below the C_{4v} structure. For the Ag_4Na^- cluster, the MP2/TZVPP, CCSD/TZVPP, and CCSD(T)/TZVPP isomer energy differences are 3.0, 28.0, and 18.8 kJ/mol with the planar isomer below the pyramidal one. The use of QZVPP quality basis sets would most likely switch the order yielding the lowest energy for the pyramidal isomers as for the corresponding Cu clusters.

The Au_4Li^- and Au_4Na^- clusters were optimized at the MP2 level using the 7s5p3d2f basis set for Au and the TZVPP basis sets for Li and Na. At the MP2 level, the planar Au_4Li^-, isomer of C_{2v} symmetry is only 0.6 kJ/mol above the pyramidal one, whereas CCSD and CCSD(T) calculations yielded the lowest energy for planar isomer. The isomer energy differences obtained at the CCSD and CCSD(T) levels are 41.3 and 29.7 kJ/mol. For Au_4Na^-, the planar isomer is significantly below the pyramidal structure at all computational levels. The isomer energy differences for Au_4Na^- obtained at the MP2, CCSD, and CCSD(T) levels are 17.9, 63.1, and 49.4 kJ/mol. The lowest isomers of both Au_4Li^- and Au_4Na^- clusters are the planar ones. The energy differences between the planar and pyramidal isomers are so large that the use of larger basis sets would hardly change the order of them.

The relative isomer energies obtained at MP2, CCSD, and CCSD(T) levels are given in Table 2, and the bond distances obtained in the structure optimizations in Table 3. The optimized cluster structures of Cu_4Li_2 (D_{4h}), Cu_4Li_2 (C_{2v}), Cu_4Li^- (C_{4v}), and Au_4Na^- (C_{2v}) are shown in Figures 3a–d.

B. Comparison Between Experimental and Calculated Photoelectron Spectra. The simulated photoelectron spectra of the pyramidal and planar Cu_4Na^- clusters shown as the blue and green curves in Figure 1 were calculated at the EOMIP CCSD level. The obtained VDEs for the pyramidal (C_{4v}) Cu_4Li^- and Cu_4Na^- clusters as well as the planar (C_{2v}) Cu_4Na^- cluster are given in Table 4. The calculated photoelectron spectra are rather independent of whether Li^+ or Na^+ is used as counterion, whereas the spectra for the planar and pyramidal Cu_4Na^- isomers differ significantly. The calculated spectra of the pyramidal Cu_4Li^- and Cu_4Na^- are very similar, except for the fourth detachment channel (Table 4). However, the peak patterns of the calculated spectra of the planar and pyramidal Cu_4Na^- clusters are completely different. This structural sensitivity of photoelectron spectra provides the basis for using PES and

TABLE 3: The M−M and M−A Bond Distances (in pm) of the M_4A^- and M_4A_2 Species (M = Cu, Ag, and Au; A = Li and Na) Optimized at the MP2 Level Using the TZVPP (Li, Na, Cu, Ag) and 7s5p3d2f (Au) Basis Sets[a]

species	level	symmetry	M−M[a]	M−M[b]	M−A[c]	M−A[d]
Cu_4Li^-	MP2/TZVPP	C_{4v}	242.0		240.3	
Cu_4Na^-	MP2/TZVPP[e]	C_{4v}	242.0		275.0	
Cu_4Li^-	MP2/TZVPP	C_{2v}	243.6	235.8	248.5	244.5
Cu_4Na^-	MP2/TZVPP	C_{2v}	244.2	236.0	280.0	284.8
Ag_4Li^-	MP2/TZVPP	C_{4v}	270.6		253.6	
Ag_4Na^-	MP2/TZVPP	C_{4v}	270.1		288.9	
Ag_4Li^-	MP2/TZVPP	C_{2v}	269.6	260.6	260.8	261.7
Ag_4Na^-	MP2/TZVPP	C_{2v}	270.3	260.3	292.2	300.0
Au_4Li^-	MP2/7s5p3d2f	C_{4v}	264.3		249.1	
Au_4Na^-	MP2/7s5p3d2f	C_{4v}	263.6		282.3	
Au_4Li^-	MP2/7s5p3d2f	C_{2v}	261.1	251.4	257.5	255.7
Au_4Na^-	MP2/7s5p3d2f	C_{2v}	260.9	251.1	294.5	284.4
Cu_4Li_2	MP2/TZVPP	D_{4h}	246.1		242.8	
Cu_4Na_2	MP2/TZVPP	D_{4v}	243.8		280.8	
Cu_4Li_2	MP2/TZVPP	C_{2v}[f]	237.4	237.8	250.1	251.8
Cu_4Na_2	MP2/TZVPP	C_{2v}[g]	237.7	239.3	282.1	290.0

[a] For the planar clusters of C_{2v} symmetry, the distance between the inner and outer M atoms. [b] The distance between the two inner M atoms of the planar clusters. [c] For the planar clusters of C_{2v} symmetry, the distance between the A atom and the outer M atom of the planar clusters. [d] The distance between the A atom and the inner M atom of the planar clusters. [e] The corresponding distances obtained at the CCSD/TZVPP level are 251.7 and 280.4 pm. [f] The distance between the inner Cu atom and the Li atom at the cusp is 255.0 pm. [g] The distance between the inner Cu atom and the Na atom at the cusp is 282.0 pm.

TABLE 4: The Vertical Detachment Energies (VDE in eV) for Cu_4Li^-, Cu_4Na^-, and Au_4Na^- Calculated at the EOMIP CCSD Level as Compared to Experimental Data[a]

Cu_4Li^-	Cu_4Na^-			Au_4Na^-		
calcd	calcd			calcd		
(C_{4v})	(C_{4v})	(C_{2v})	exp	(C_{4v})	(C_{2v})	exp
1.313	1.229	1.137	1.13	2.501	2.662	2.98
3.193	3.259	2.586	3.26	3.769	3.980	4.12
3.636	3.864	3.840	3.84	4.295	4.751	4.79
4.062	3.876	3.871		4.923	4.758	4.98
		3.985		5.365	5.120	
		4.213		5.525	5.439	
				5.734	5.656	

[a] The molecular structures optimized at the MP2 level were used. The cluster symmetry is also indicated

calculations to determine cluster structures. We were not able to measure the photoelectron spectra of Cu_4Li^- because of its complicated isotope pattern. Our measured photoelectron spectra of Cu_4Na^- (the red curves in Figure 1) are in good agreement with the simulated spectrum for the pyramidal structure (the blue curve) but disagree with the simulated spectrum for the planar structure (the green curve). In particular, the second detachment channel for the planar structure with a calculated VDE at 2.586 eV has no corresponding peak in the experimental spectrum. The comparison between the calculated and measured photoelectron spectra suggests that the experimental spectra are due to the Cu_4Na^- cluster of C_{4v} symmetry, consisting of a planar four-membered Cu_4^{2-} ring. The planar Cu_4Na^- isomer of C_{2v} symmetry can be ruled out to be the main contributor to the experimental spectra since its second VDE deviates by 0.66 eV from the experimental value (Table 4) and the estimated uncertainty of the VDE calculated at the EOMIP CCSD/TZVPP level is significantly smaller.[35]

The calculated photoelectron spectra of the planar (C_{2v}) and pyramidal (C_{4v}) isomers of Au_4Na^- at the EOMIP CCSD level

(a) $11e_u$ (-5.33)   (b) $9a_{1g}$ (-9.71)

Figure 4. The HOMO (a) and HOMO-1 (b) molecular orbitals of Cu_4-Li_2 calculated at the Hartree−Fock self-consistent field (HF SCF/TZVPP) level using the MP2/TZVPP molecular structure. The orbitals are spectated along the C_4 axis. The orbital energies (in eV) are given within parentheses. The pictures have been made using gOpenMol [43,-44].

are shown in Figure 2, and the obtained ionization potentials are compared with the experimental VDEs in Table 4. Clearly, the calculated spectral pattern of the planar isomer (the green curve in Figure 2) agrees well with the experimental spectra (the red curves), although the calculated VDEs are somewhat smaller than the observed ones (Table 4). On the other hand, the pattern of the calculated photoelectron spectra for the pyramidal Au_4Na^- cluster (the blue curve in Figure 2) differs significantly from that of the experimental spectrum. These observations are consistent with the energetics of the two Au_4Na^- isomers and confirm that the planar Au_4Na^- isomer is indeed the global minimum.

C. The Nature of the Aromaticity of the Square-Planar Cu_4^{2-} Unit. Wannere et al.[18] calculated nucleus independent chemical shifts (NICS) for bipyramidal Cu_4Li_2, Ag_4Li_2, and Au_4Li_2. On the basis of the NICS contributions from different orbitals, they concluded that the aromatic properties of these clusters possess distinct differences from other square ring systems such as Al_4Li_2. According to their NICS calculations, the coinage four-membered rings are stabilized by d orbital aromaticity i.e., the cyclic electron delocalization is due to d electrons rather than p electrons as in ordinary aromatic molecules, because they found that the diamagnetic NICS value of -14.5 ppm at the center of the cluster seems to originate from MOs with significant $3d$ character. The self-canceling orbital contributions in the NICS treatment is probably an artifact due to an unphysical orbital decomposition.[36] A comparison of the nuclear magnetic shielding constants for the Cu atoms, $\sigma(Cu)$, calculated at ab initio and DFT levels of theory also indicates that generalized gradient (GGA) DFT methods should not be used to assess the aromaticity properties of the Cu_4^{2-} species. Calculations of the nuclear magnetic shielding constants (σ) for Cu_4Li_2 at the DFT level using Becke's three-parameter hybrid functional (B3LYP)[37,38] yield $\sigma(Cu)$ values which are 600 ppm (67%) larger than the shielding constants obtained at the BP86 GGA level.[39−41] The $\sigma(Cu)$ values calculated at the HF/TZVPP, MP2/TZVPP, and CCSD/TZVPP levels are 1838, 1675, and 1690 ppm, respectively, as compared to the B3LYP/TZVPP and BP86/TZVPP values of 1473 and 881 ppm. The small $\sigma(Cu)$ value obtained in the BP86 GGA DFT calculation indicates that GGA DFT calculations are not recommended for studies of the magnetic shieldings of the Cu_4^{2-} clusters, whereas the Hartree-Fock-based ab initio correlation methods (MP2 and CCSD) seem to yield consistent nuclear magnetic shieldings.

The orbital plot in Figure 4 shows that the a_{1g} orbital has a large amplitude at the center of the Cu_4Li_2 cluster. The presence of a significant amount of electron charge at the cluster center shields the external magnetic field in the NICS point. Thus, the diamagnetic shielding contribution from the a_{1g} orbital in the NICS point is due to the presence of its electrons and not due to ring currents sustained by it. However, the highest
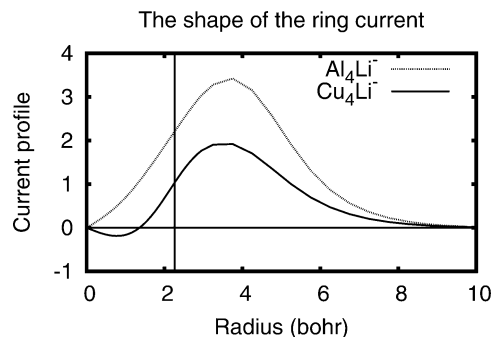

Figure 5. The shape of the ring current (in nA/T/bohr) for Cu_4Li^- calculated at the CCSD/TZVPP level using the MP2/TZVPP molecular structure is compared to the ring current profile of the Al_4^{2-} ring [14]. The vertical bar denotes the size of the Cu_4^{2-} ring. The size of the Al_4^{2-} ring is 0.2 bohr greater.

TABLE 5: The Integrated Ring-Current Susceptibilities (in nA/T) for Cu_4Li^-, Cu_4Li_2, and Cu_4H_4 Calculated at the CCSD/TZVPP Level Using the GIMIC Method

	$Al_4Li^{-\ a}$	Cu_4Li^-	Cu_4Li_2	Cu_4H_4
diamagnetic current	32.4	19.4	23.2	2.1
paramagnetic current	0.0	−0.4	−0.4	−2.7
total current	32.4	19.0	22.8	−0.6
contribution from Li[b]	4.3	6.4	12.9	−
total ring current	28.1	12.6	10.0	−0.6

a From ref 14. *b* The estimated net current circling the Li^+ cations.

occupied molecular orbital (HOMO) belonging to the e_u irreducible representation is ring-shaped and has a significant amplitude outside the Cu_4^{2-} ring. The orbital pictures suggest that the HOMO is sustaining the current and therefore responsible for the aromaticity properties of the Cu_4^{2-} ring.

The first-order magnetically induced current density for Cu_4Li^- was calculated at the CCSD/TZVPP level using the GIMIC method.[16] In Figure 5, the shape of the magnetically induced ring current passing on the open side of the Cu_4Li^- ring is compared to the corresponding curve for Al_4Li^-. The current profiles of the two species are strikingly similar. The main difference between the Cu_4^{2-} and Al_4^{2-} currents is that for Cu_4^{2-} the current in the interior of the molecular ring is weak and dominantly paramagnetic, whereas for Al_4^{2-} the ring current is diatropic both inside and outside the ring. The a_{1g} orbital (HOMO-1) of Cu_4Li^- which has large amplitudes inside the ring does apparently not sustain any strong ring current. The large ring current appearing outside the Cu_4^{2-} ring suggests that the e_u orbital (HOMO) is mainly responsible for the transport of the electrons.

The integrated ring-current strengths passing a radial cross section are given in Table 5. The ring-current susceptibilities of 12.6 and 10.0 nA/T for Cu_4Li^- and Cu_4Li_2, respectively, are about as large as in benzene.[16,42] The ring-current susceptibility of the Cu_4^{2-} ring is thus 2−3 times weaker than for the Al_4^{2-} species.

The explicit orbital contributions to the magnetically induced currents cannot be obtained using the GIMIC method, because orbital currents are dependent on the choice of the gauge origin[36] and the unphysical current contributions from mixing of occupied orbitals cannot be eliminated in the GIMIC scheme. The contribution from valence s orbitals was therefore estimated by removing them from the basis set. In the current calculations without valence s orbitals, the ring-current susceptibility obtained at the MP2 level is 4.0 nA/T as compared to the MP2/TZVPP value of 12.2 nA/T; the Cu_4^{2-} ring sustains a weak ring current when the valence s basis functions are absent.
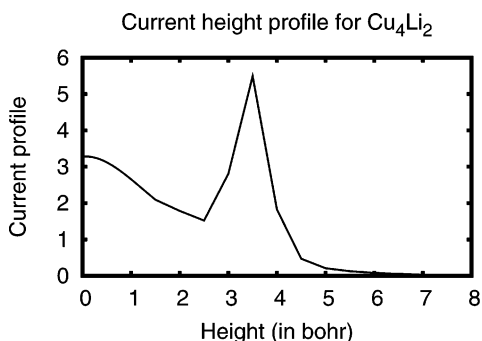
Alkali-Metal Coinage-Metal Clusters

J. Phys. Chem. A, Vol. 110, No. 12, 2006 **4249**

Current height profile for Cu₄Li₂

Figure 6. The current profile (in nA/T/bohr) as a function of the vertical distance from the Cu_4^{2-} ring in Cu_4Li_2 calculated at the CCSD/TZVPP level using the MP2/TZVPP structure.

The GIMIC calculation of the vertical current profile in Figure 6 shows that the current in Cu_4Li_2 is not only sustained in the ring plane, but also between the ring and the Li^+ counterions. The sharp peak at 3.5 bohr is due to the Li^+ cations. The GIMIC calculations of the current density of Cu_4Li^- show that Cu_4^{2-} can be considered to be σ aromatic. In contrast to Wannere et al.,[18] we find no need to invoke the d-orbitals in order to explain the aromaticity of planar four-membered Cu_4^{2-} rings. In the case of Au_4Na^-, the calculations show that the planar isomer of C_{2v} symmetry is the energetically lowest one. This is also in agreement with experiment, since the measured photoelectron spectra indicates that the planar Au_4Na^- is also observed experimentally.

The magnetically induced current density was also calculated for Cu_4H_4, which is a planar molecule consisting of a square-shaped Cu_4 ring with the hydrogens bridging around it at the edges. As seen in Table 5, the Cu_4 ring in Cu_4H_4 does not sustain any strong magnetically induced ring current. The weak diatropic current circles inside and outside the Cu_4 ring, whereas the region in the vicinity of the H atoms and outside them are dominated by the paratropic ring current. The net ring-current susceptibility for Cu_4H_4 is only -0.6 nA/T.

V. Conclusions

Two coinage and alkali metal mixed clusters (Cu_4Na^- and Au_4Na^-) produced with laser vaporization have been characterized experimentally using photoelectron spectroscopy and computationally at correlated ab initio levels. The comparison of measured and calculated photoelectron spectra shows that the observed Cu_4Na^- cluster is a pyramidal species with C_{4v} symmetry, whereas the observed Au_4Na^- cluster is planar with C_{2v} symmetry.

Ab initio electron correlation calculations also predict the pyramidal Cu_4Na^- and the planar Au_4Na^- isomers to be the energetically lowest ones. At the CCSD(T)/$7s5p3d2f$ level, the planar Au_4Na^- isomer lies 49.4 kJ/mol below the pyramidal one, whereas at extrapolated CCSD(T)/QZVPP level, the pyramidal Cu_4Na^- cluster lies 16.9 kJ/mol below the planar one. Ab initio calculations on Ag_4Li^- and Ag_4Na^- show that the energetics of the Ag_4^{2-} clusters are similar to those of the Cu_4^{2-} species. The pyramidal Ag_4Li^- and Ag_4Na^- clusters are thus most likely the global minima.

Calculations of the magnetically induced current density in pyramidal Cu_4Li^- (C_{4v}) and bipyramidal Cu_4Li_2 (D_{4h}) clusters using the Gauge-Including Magnetically Induced Current (GIMIC) method show that the strong ring current is sustained mainly by the highest-occupied molecular orbital dominated by Cu $4s$ character. The Cu_4^{2-} ring is σ aromatic mainly from the $4s$ bonding interactions and the d orbitals do not sustain any strong

ring current. The aromatic character of Cu_4^{2-} can thus be explained in terms of σ aromaticity. We found no evidence of any significant current density being sustained by the d-orbitals.

Supporting Information Available: The atomic coordinates are given for the molecular structures of Cu_4Li^-, Cu_4Na^-, Ag_4Li^-, Ag_4Na^-, Au_4Li^-, Au_4Na^-, Cu_4Li_2, Cu_4Na_2, Ag_4Li_2, Ag_4Na_2, Au_4Li_2, and Au_4Na_2 optimized at the MP2 level using the TZVPP (Cu, Ag, Li, and Na) and $7s5d3d2f$ (Au) basis sets. The total energies (in a.u.) calculated at HF, MP2, CCSD, and CCSD(T) levels are also reported. This material is available free of charge via the Internet at http://pubs.acs.org.

References and Notes

(1) Li, X.; Kuznetsov, A. E.; Zhang, H. F.; Boldyrev, A. I.; Wang, L. S. *Science* **2001**, *291*, 859.

(2) Kuznetsov, A. E.; Birch, K. A.; Boldyrev, A. I.; Li, X.; Zhai, H. J.; Wang, L. S. *Science* **2003**, *300*, 622.

(3) Kuznetsov, A. E.; Corbett, J. D.; Wang, L. S.; Boldyrev, A. I. *Angew. Chem., Int. Ed.* **2001**, *40*, 3369.

(4) Boldyrev, A. I.; Kuznetsov, A. E. *Inorg. Chem.* **2002**, *41*, 532.

(5) Kuznetsov, A. E.; Boldyrev, A. I.; Li, X.; Wang, L. S. *J. Am. Chem. Soc.* **2001**, *123*, 8825.

(6) Li, X.; Zhang, H. F.; Wang, L. S.; Kuznetsov, A. E.; Cannon, N. A.; Boldyrev, A. I. *Angew. Chem., Int. Ed.* **2001**, *40*, 1867.

(7) Boldyrev, A. I.; Wang, L. S. *Chem. Rev.* **2005**, *105*, 3716.

(8) Heine, T.; Corminboeuf, C.; Seifert, G. *Chem. Rev.* **2005**, *105*, 3889.

(9) Jusélius, J.; Straka, M.; Sundholm, D. *J. Phys. Chem. A* **2001**, *105*, 9939.

(10) Fowler, P. W.; Havenith, R. W. A.; Steiner, E. *Chem. Phys. Lett.* **2001**, *342*, 85.

(11) Zhan, C.-G.; Zheng, F.; Dixon, D. A. *J. Am. Chem. Soc.* **2002**, *124*, 14795.

(12) Chen, Z.; Corminboeuf, C.; Heine, T.; Bohmann, J.; von Ragué Schleyer, P. *J. Am. Chem. Soc.* **2003**, *125*, 13930.

(13) Havenith, R. W. A.; Fowler, P. W.; Steiner, E.; Shetty, S.; Kanhere, D.; Pal, S. *Phys. Chem. Chem. Phys.* **2004**, *6*, 285.

(14) Lin, Y. C.; Jusélius, J.; Sundholm, D.; Gauss, J. *J. Chem. Phys.* **2005**, *122*, 214308.

(15) von Ragué Schleyer, P.; Maerker, C.; Dransfeld, A.; Jiao, H.; van Eikema Hommes, N. J. R. *J. Am. Chem. Soc.* **1996**, *118*, 6317.

(16) Jusélius, J.; Sundholm, D.; Gauss, J. *J. Chem. Phys.* **2004**, *121*, 3952.

(17) Ritter, S. K. *Chem. Eng. News* **2003**, *81* (50), 23.

(18) Wannere, C. S.; Corminboeuf, C.; Wang, Z. X.; Wodrich, M. D.; King, R. B.; von Ragué Schleyer, P. *J. Am. Chem. Soc.* **2005**, *127*, 5701.

(19) Fuentealba, P.; Padilla-Campos, L. *Intern. J. Quantum Chem.* **2005**, *102*, 498.

(20) Tsipis, A. C.; Tsipis, C. A. *J. Am. Chem. Soc.* **2003**, *125*, 1136.

(21) Tsipis, A. C.; Karagiannis, E. E.; Kladou, P. F.; Tsipis, C. A. *J. Am. Chem. Soc.* **2004**, *126*, 12916.

(22) Wang, L. S.; Cheng, H. S.; Fan, J. *J. Chem. Phys.* **1995**, *102*, 9480.

(23) Wang, L. S.; Wu, H. in *Advances in Metal and Semiconductor Clusters: Cluster Materials*; Duncan, M. A., Ed.; JAI Press: Greenwich, CT, 1998; pp 299−343.

(24) Ahlrichs, R.; Bär, M.; Häser, M.; Horn, H.; Kölmel, C. *Chem. Phys. Lett.* **1989**, *162*, 165, current version: see http://www.turbomole.de.

(25) Gilb, S.; Weis, P.; Furche, F.; Ahlrichs, R.; Kappes, M. M. *J. Chem. Phys.* **2002**, *116*, 4094.

(26) Pyykkö, P.; Runeberg, N.; Mendizabal, F. *Chem. Eur. J.* **1997**, *3*, 1451.

(27) The optimized *p* exponent of 0.80896058156 was used. The exponents of the *f* functions were 1.19 and 0.43023309776.[25]

(28) Andrae, D.; Häussermann, U.; Dolg, M.; Stoll, H.; Preuss, H. *Theor. Chim. Acta* **1990**, *77*, 123.

(29) Stanton, J. F. *J. Chem. Phys.* **1994**, *101*, 8938.

(30) Stanton, J. F.; Gauss, J.; Watts, J. D.; Lauderdale, W. J.; Bartlett, R. J. *Intern. J. Quantum Chem. Symp.* **1992**, *26*, 879, current version: see http://www.aces2.de.

(31) Gauss, J. *Chem. Phys. Lett.* **1992**, *191*, 614.

(32) Gauss, J. *J. Chem. Phys.* **1993**, *99*, 3629.

(33) Gauss, J.; Stanton, J. F. *J. Chem. Phys.* **1995a**, *102*, 251.

(34) Gauss, J.; Stanton, J. F. *J. Chem. Phys.* **1995b**, *103*, 3561.

(35) Stanton, J. F.; Sattelmeyer, K. W.; Gauss, J.; Allan, M.; Skalicky, T.; Bally, T. *J. Chem. Phys.* **2001**, *115*, 1.

(36) Steiner, E.; Fowler, P. W. *Phys. Chem. Chem. Phys.* **2004**, *6*, 261.

(37) Becke, A. D. *J. Chem. Phys.* **1993**, *98*, 5648.

(38) Lee, C.; Yang, W.; Parr, R. G. *Phys. Rev. B* **1988**, *37*, 785.

(39) Vosko, S. H.; Wilk, L.; Nusair, M. *Can. J. Phys* **1980**, *58*, 1200.

(40) Perdew, J. P. *Phys. Rev. B* **1986**, *33*, 8822.

(41) Becke, A. D. *Phys. Rev. A* **1988**, *38*, 3098.

(42) Johansson, M. P.; Jusélius, J.; Sundholm, D. *Angew. Chem., Int. Ed.* **2005**, *44*, 1843.

(43) Laaksonen, L. *J. Mol. Graphics* **1992**, *10*, 33, current version: see http://www.csc.fi/gopenmol.

(44) Bergman, D. L.; Laaksonen, L.; Laaksonen, A. *J. Mol. Graphics Modell.* **1997**, *15*, 301.